First published in: Proceedings of the Europan Conference on Antennas and Propagation EuCAP 2009

Performance of Wavefront Migration Imaging in the Near Field of the Antennas

Malgorzata Janson, Grzegorz Adamiuk, Thomas Zwick, and Werner Wiesbeck

Institut für Höchstfrequenztechnik und Elektronik, Universität Karlsruhe (TH)
Kaiserstr 12, 76131 Karlsruhe, Germany
malgorzata.porebska@ihe.uka.de

***Abstract*— The performance of an ultra wideband (UWB) imaging system has been studied for targets placed in the near field of the antennas. The targets in the proximity of antennas are causing additional coupling between the antennas and thus the distortion of transmitted pulses. As the most algorithms for UWB imaging utilize the information about the shape and delay of the received pulses the distortions may influence the quality of the image. The degree of pulse distortion depends on the size of the target, its material properties and distance to the antennas. It is shown that it is possible to obtain the image of the target already at small distances even if some signal distortion due to the coupling occurs.**

I. Introduction

Ultra wideband (UWB) technology recently became a topic of great interest and attracts a growing number of researchers. UWB systems utilize an extremely large bandwidth (absolute bandwidth $> 500\,\mathrm{MHz}$ or relative bandwidth $> 20\%$), which allows for high data rates and precise imaging. Due to approval of unlicensed operation of UWB systems by the Federal Communications Commission (FCC) in 2002 [1] and by the European Commission in 2007 [2] the way for the commercial applications using UWB has been opened.

While the high-rate communication systems seem to be the main application of UWB also localization and radar systems can profit from the fine time resolution resulting from the extremely large bandwidth [3]. In this paper the wavefront migration algorithm for imaging described in [4], [5], [6] is considered. The algorithm uses the information about signal shape and time delay of the signal at the receive antenna to create an image of the scenario in front of the imaging system.

The quality of the image depends on the shape of received signal. Targets placed in the near field of the antennas cause additional coupling and may distort the signal. In this paper the influence of such targets on the image is analyzed using the Finite Integral Method provided by CST Microwave Studio©.

The remainder of this papers is organized as follows: First the description of the used imaging approach and of used scenario is given. Then simulation results are presented and conclusions are drawn.

II. Imaging approach

The imaging method under consideration is the time domain migration [4], [5], [6]. In this method the sensor consisting of a transmit (Tx) and a receive (Rx) antenna is moved along a linear route. At each position the scattered data are recorded. Assuming that an ideal point scatterer is present in the considered area, the sent pulse will be delayed by the time corresponding to the forward and return way of the signal. With changing position of the sensor the delay of the received pulse changes, causing a hyperbolic wave front in the collected data.

The information about the delay at each particular sensor position allows to construct an ellipse with the foci at the positions of Tx and Rx. The length of the semimajor axis corresponds to the delay of the signal. In the monostatic case, when the Tx and Rx are co-positioned the ellipse is replaced by a circle. This ellipse corresponds to all possible positions of the scatter. The ellipses for all sensor positions have a common point at the real position of the scatterer (cf. Fig. 1).

An image of the whole considered area can be obtained in a following way: first a grid for the image $O(x, y)$ is generated for the area under consideration. For each point of the grid a point scatterer is assumed, and the distance between this scatterer and the sensor is calculated. Then the values of the measured data are found for this distance. Repeating this procedure for all antenna positions delivers the final image. This is expressed by following equation:

$$O(x,y) = \sum_{n=1}^{N} h_n \left(\frac{r_{Tx_n} + r_{Rx_n}}{c} \right) \tag{1}$$

where h_n is the impulse response measured at the n-th receiver position. r_{Tx_n} is the distance between the transmitter and the considered scatterer and r_{Rx_n} is the distance between the scatterer and the receiver. c indicates the velocity of light.

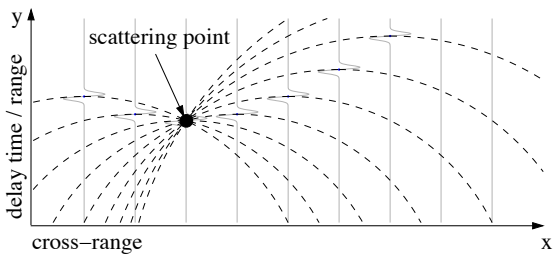

Fig. 1. Time domain migration principle (monostatic case)

III. Simulation scenario

To asses the influence of the near field coupling between the antennas and the target on the results of the imaging, following scenario has been considered: Two Vivaldi antennas with dimensions 78×80 mm are placed 15 cm apart (cf. Fig. 2). In the front of the antennas targets comprising a PEC (Perfect Electric Conductor) cylinder with radius of 2 cm, a PEC cylinder with radius of 0.5 cm and a thin PEC plate of dimensions 30×20 cm are placed at different distances d to the front edge of the antennas.

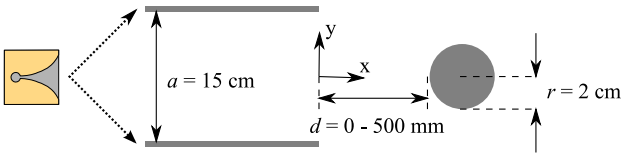

Fig. 2. Simulation scenario

The distances d between the antennas and the targets are chosen so that near field and far field are covered. The lower limit of the far field of an antenna is dependent on its dimensions and frequency [7]:

$$d_{\text{ff}} > 2D^2/\lambda_0, \tag{2}$$

where D is the largest dimension of the antenna and λ_0 is the wavelength. In the UWB case the large bandwidth results in large differences between minimal and maximal distances, at which the far field is expected. For the FCC band (3.1 GHz to 10.6 GHz) the minimal far field distance of the Vivaldi antennas is 13 cm (at 3.1 GHz) and the maximal one is 45 cm (at 10.6 GHz).

To perform the migration at a given distance d the antenna system is shifted in 2.5 cm steps along y-axis from the position $y = -0.5$ m to the position $y = 0.5$ m. At each position a transmission of a Gaussian pulse is simulated with CST Microwave Studio©. The direct coupling between the antennas is calibrated out using a simulation of transmission between both antennas in the free space. Also the impulse response of the antennas is deconvolved from the received signal using a simulated impulse response in the direction of the antenna main beam. The processed data is used as an input of the imaging algorithm described in section II.

IV. Simulation results

First the pulse shapes for the considered targets placed at the x-axis ($y = 0$) are investigated at different distances d. In the Fig. 3 the received signals scattered from the targets are presented. The amplitude of the pulses is normalized with respect to the maximum of each pulse. For better comparison a time window of 1 ns around the maximum of the pulse is shown in each subfigure.

The pulses scattered at the targets in the proximity of the antennas have irregular shapes due to coupling between antennas and target. The further is the target from antennas the more is the pulse shape similar to the pulse shape in the

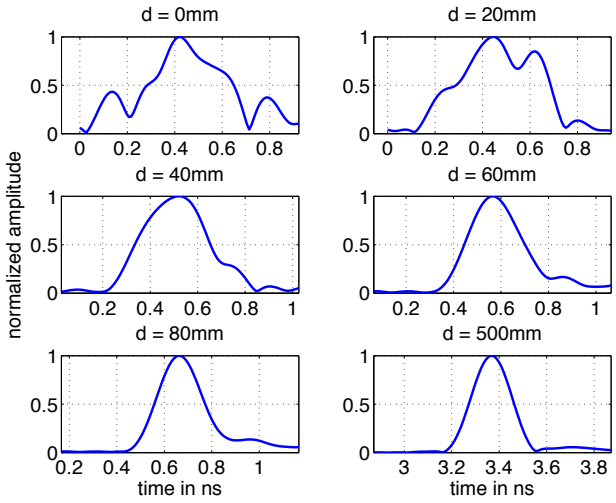

(a) PEC cylinder $r = 2$ cm

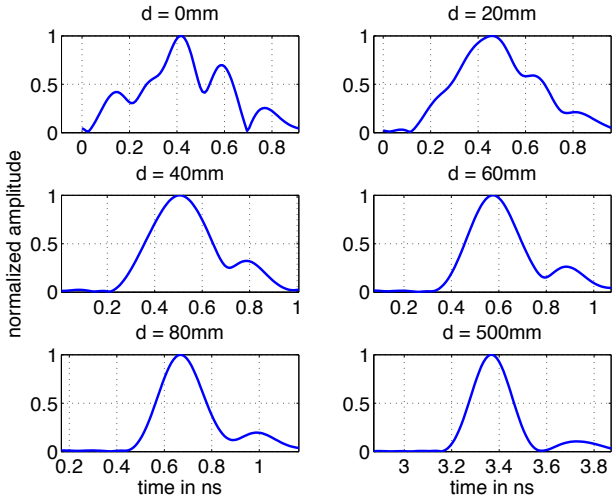

(b) PEC cylinder $r = 0.5$ cm

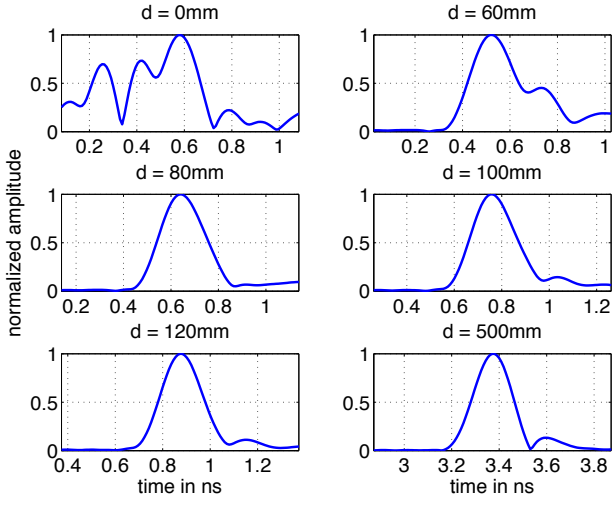

(c) PEC plate

Fig. 3. Pulse shapes for different PEC targets

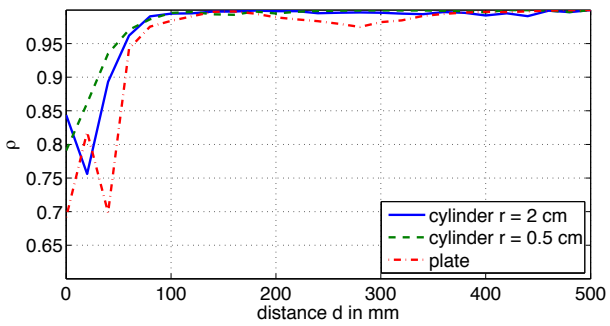

Fig. 4. Correlation coefficient between received signal at the distance d and the far field signal

far field. The similarity of two signals is often described by the correlation coefficient. In Fig. 4 the correlation coefficient between the received signal at given distance d and the received signal in far field (at the distance $d = 500\,\text{mm}$) is shown. The correlation coefficients become higher than 0.95 for distances of ca. 60 mm from the antennas edges for all considered objects. The corresponding images at the distances d of 20, 60 and 500 mm are shown in Fig. 5.

The irregular pulses observed for small distances between the target and the antennas result in an deformed migrated image, as it can be seen in Fig. 5(a), 5(b) and 5(c). The target is not recognizable at this distance. On the other side at the distance $d = 60\,\text{mm}$, at which the pulse shape is more similar to the pulse shape in the far field also the target images (Fig. 5(d), 5(e) and 5(f)) become similar to the images in the far field (Fig. 5(g), 5(h) and 5(i)).

The circular artifacts visible in the images at the distances of 60 mm and 20 mm arise from the ellipses generated by the algorithm for each antenna position. They are present also in the images of the targets in the far field but their radii rise with the distance of the target to the antennas. The amplitude of these artifacts falls with rising number of considered sensor positions. For the considered targets and sensor track length (1 m) the image with no considerable artifacts can be obtained for the spacing of 1.25 cm between the sensor positions.

The coupling between the target and the antennas influences also the amplitude and the delay of the pulses. Fig. 6 shows the amplitudes of the received pulses for the targets at different distances. For small distances d the pulse amplitude rises with the distance, then it falls as expected for the far field. The distances, at which the pulse amplitudes begin to decrease with the distance are ca. 12 cm for both cylinders and 14 cm for the plate.

The influence of the coupling between the target and the antennas on the delay of the received pulses has been found to be small for all distances. This means that the delay of the pulses does not vary significantly from the theoretical delay resulting from the spacing between the target and the

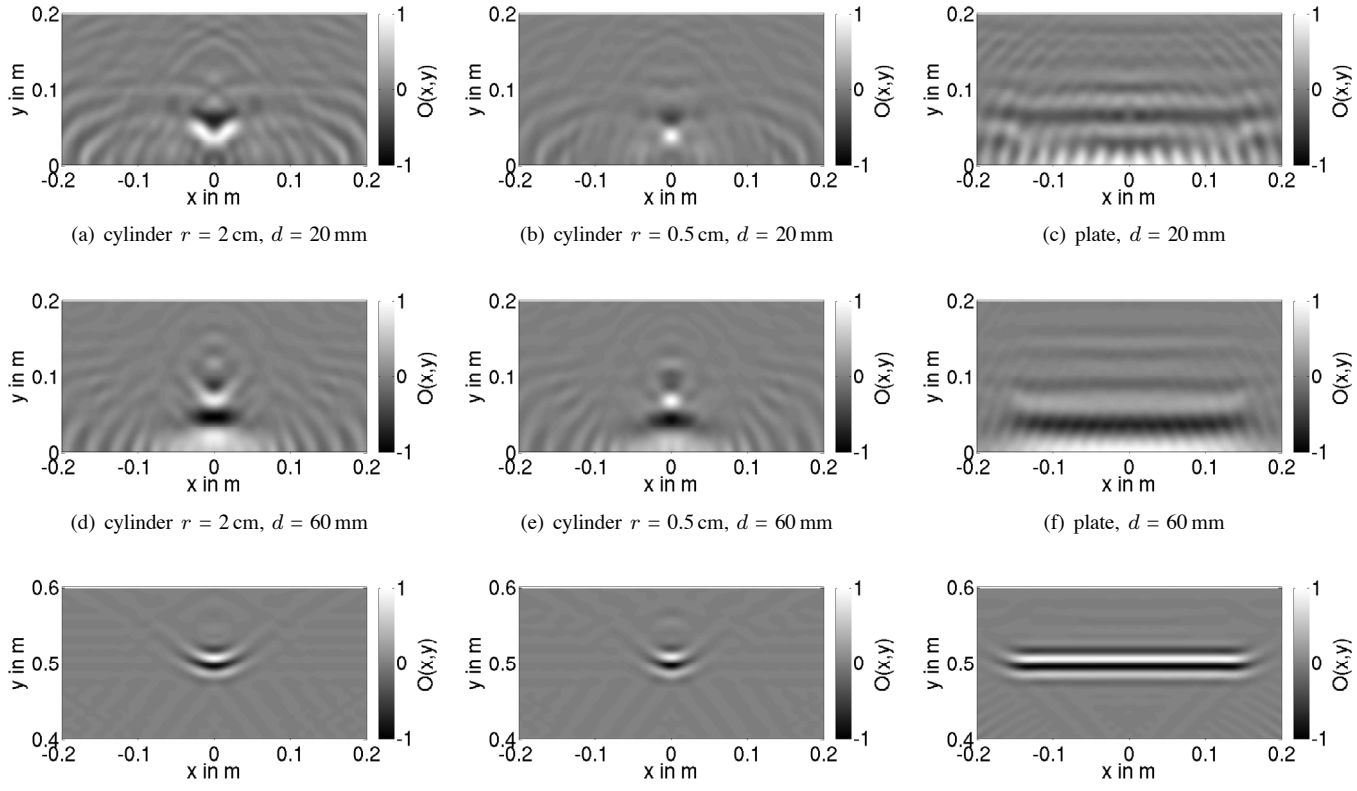

(a) cylinder $r = 2\,\text{cm}$, $d = 20\,\text{mm}$ (b) cylinder $r = 0.5\,\text{cm}$, $d = 20\,\text{mm}$ (c) plate, $d = 20\,\text{mm}$

(d) cylinder $r = 2\,\text{cm}$, $d = 60\,\text{mm}$ (e) cylinder $r = 0.5\,\text{cm}$, $d = 60\,\text{mm}$ (f) plate, $d = 60\,\text{mm}$

(g) cylinder $r = 2\,\text{cm}$, $d = 500\,\text{mm}$ (h) cylinder $r = 0.5\,\text{cm}$, $d = 500\,\text{mm}$ (i) plate, $d = 500\,\text{mm}$

Fig. 5. Migrated images of the considered targets

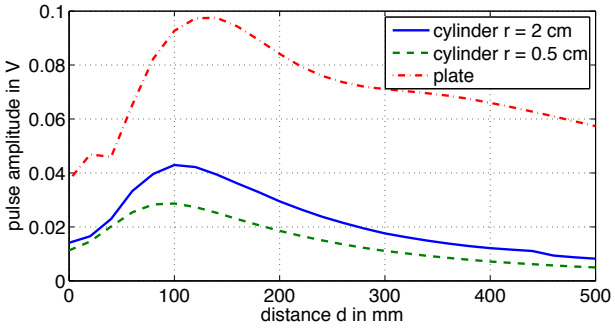

Fig. 6. Pulse amplitude at distance d

antennas. The error between the delay of simulated pulse and the theoretical delay, calculated from the scenario geometry has been found to be in order of 100 ps for the very near targets (d up to ca. 60 mm) and to fall for larger distances.

In practice the scattered signals from the objects at the distances $d \leq a/2$ are hard to extract from the measured data because the signal delay of direct and scattered signal are roughly the same. In the simulations above the conditions for the configuration with and without target are exactly the same, so the direct coupling between antennas can be subtracted from the received signal. In the case of real measurements it may not be possible to extract the direct signal completely. Thus the performance of imaging system for very near targets is limited at this distance provided that no measures for the reduction of the direct coupling have been taken.

V. Conclusions

The influence of the targets in the near field of antennas has been found to be limited to very small distances. Only for distances of few cm between the targets and the antennas the image is heavily distorted. Already at distances of ca. 6 cm was it possible to obtain an image of the target, even though the target is in the near field of the considered antennas. The comparison of the pulse shapes for different distances and targets reveal the dependency on the target size. However, the differences in the minimal imaging distance for the considered objects of different sizes are very small.

References

[1] *Revision of Part 15 of the Comission's Rules Regarding Ultra Wideband - First Report and Order 02-48*, Federal Communications Comission (FCC), 2002.

[2] *Decision 2007/131/EC on allowing the use of the radio spectrum for equipment using ultra-wideband technology in a harmonised manner in the Community*, European Commission, Feb. 2007.

[3] S. Gezici, Z. Tian, G. Giannakis, H. Kobayashi, A. Molisch, H. Poor, and Z. Sahinoglu, "Localization via ultra-wideband radios: a look at positioning aspects for future sensor networks," *IEEE Signal Processing Magazine*, vol. 22, no. 4, pp. 70–84, 2005.

[4] D. Daniels, *Ground penetrating Radar*, 2nd ed. London: Institution of Electrical Engineers, 2006.

[5] S. Hantscher, B. Praher, A. Reisenzahn, and C. Diskus, "Comparison of UWB target identification algorithms for through-wall imaging applications," in *3rd European Radar Conference, EuRAD 2006, Manchester, GB*, Sept. 2006, pp. 104–107.

[6] R. Zetik, J. Sachs, and R. Thomä, "Imaging of propagation environment by UWB channel sounding," in *XXVIIIth General Assembly of URSI, New Delhi, India*, Oct. 2005.

[7] C. Balanis, *Antenna Theory: Analysis and Design*. John Wiley & Sons, Inc., New Jersey, 2005.